Electronic Supplementary Material (ESI) for Dalton Transactions.
This journal is © The Royal Society of Chemistry 2015

Targeting Divalent Metal Cations with Re(I) Tetrazolato Complexes

Valentina Fiorini,[a] Anna Maria Ranieri,[a] Sara Muzzioli,[a] Karen D. M. Magee,[b] Stefano Zacchini,[a] Nurshadrina Akabar,[b] Alessandra Stefan,[c] Mark I. Ogden,[b] Massimiliano Massi,*[b] Stefano Stagni*[a]

[a]*Department of Industrial Chemistry "Toso Montanari", University of Bologna, Viale Risorgimento 4, I-40136 Bologna, Italy*

[b] *Nanochemistry Research Institute, Department of Chemistry, Curtin University, GPO Box U 1987, Perth, Australia, 6845*

[c]*Department of Pharmacy and Biotechnology, University of Bologna, Viale Risorgimento 4, I-40136 Bologna, Italy*

e-mail: stefano.stagni@unibo.it (Stefano Stagni), m.massi@curtin.edu.au (Massimiliano Massi)

SUPPORTING INFORMATION

Infrared Spectroscopy

Table S1. Stretching frequencies (cm^{-1}) of the CO bands of all the Re(I) complexes reported in this work. Values are relative to solution state (dichloromethane as the solvent) IR spectra were recorded at room temperature.

Complex	CO A'(1)	CO A'(2)/A''
***fac*-[Re(phen)(CO)$_3$(2-PTZ)]**	2030	1923
***fac*-[Re(bipy)(CO)$_3$(2-PTZ)]**	2028	1923
[Re-(2-PTZ)-Cu]$^+$	2031	1925
***fac*-[Re(phen)(CO)$_3$(2-QTZ)]**	2033	1922
***fac*-[Re(bipy)(CO)$_3$(2-QTZ)]**	2032	1922
[Re-(2-QTZ)-Cu]$^+$	2032	1927

NMR (^{1}H, ^{13}C) Spectra

Figure S1. *fac*-[Re(**phen**)$(CO)_3$(**2-QTZ**)]: ^{1}H-NMR spectrum **(**Acetone-*d*^{6}*,* 400 MHz, r.t.).

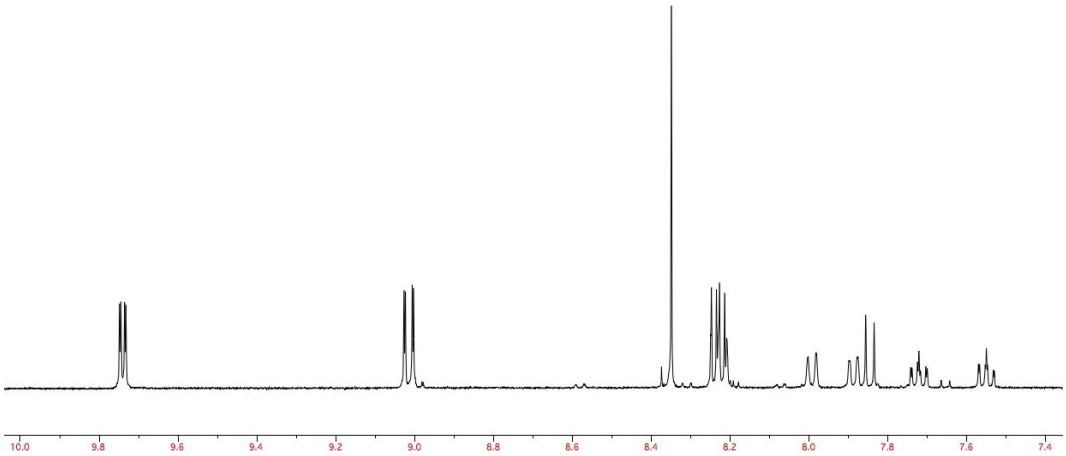

Figure S2. *fac*-[Re(**phen**)$(CO)_3$(**2-QTZ**)] : ^{13}C-NMR spectrum **(**DMSO-*d*^{6}*,* 100 MHz, r.t.).

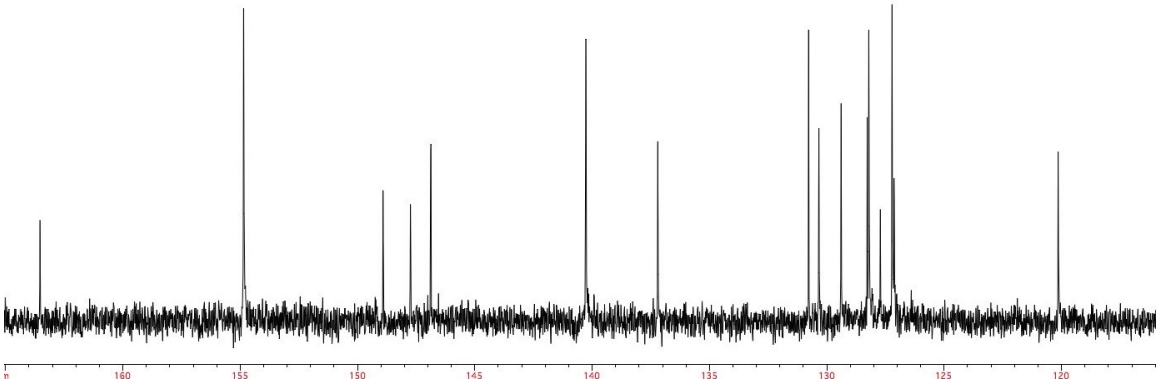

Figure S3. *fac*-[Re(**bipy**)$(CO)_3$(**2-QTZ**)]: ^{1}H-NMR spectrum **(**Acetone-*d*^{6}, 400 MHz, r.t.).

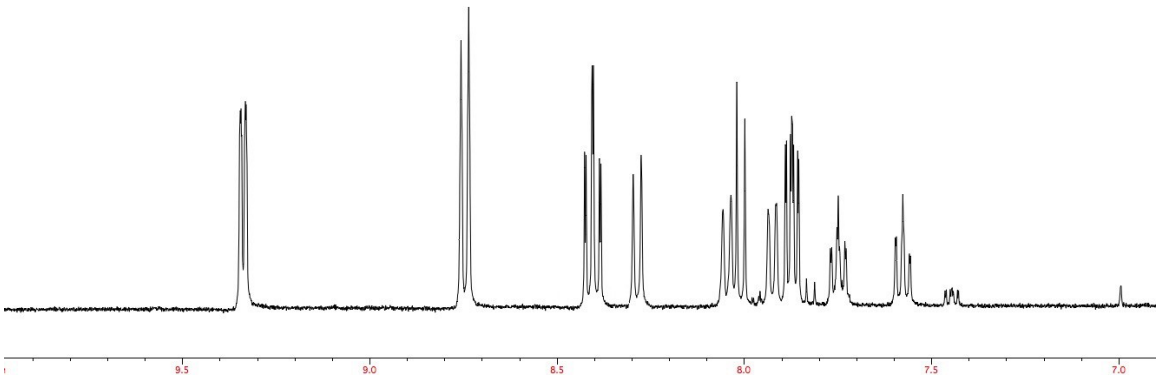

Figure S4. *fac*-[Re(**bipy**)$(CO)_3$(**2-QTZ**)]: ^{13}C-NMR spectrum **(**DMSO-*d*^{6}, 100 MHz, r.t.).

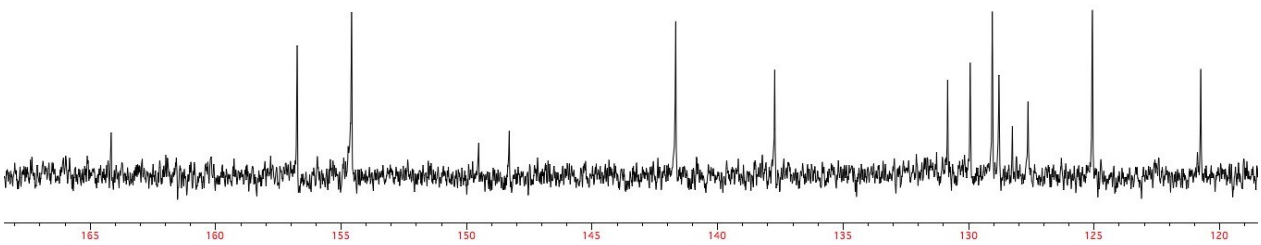

Figure S5. *fac*-[Re(**phen**)$(CO)_3$(**2-PTZ**)]: ^{1}H-NMR spectrum **(**DMSO-d^6, 400 MHz, r.t.).

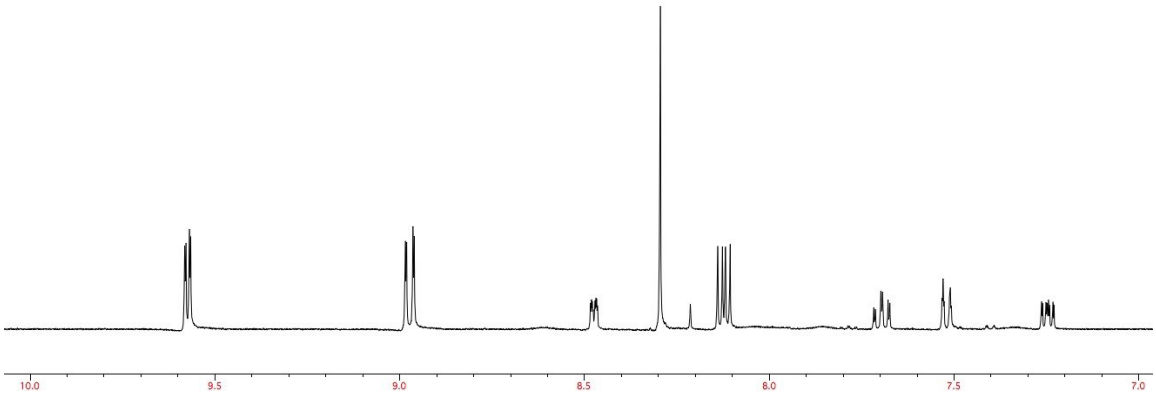

Figure S6. *fac*-[Re(**phen**)$(CO)_3$(**2-PTZ**)]: ^{13}C-NMR spectrum **(**DMSO-d^6, 100 MHz, r.t.).

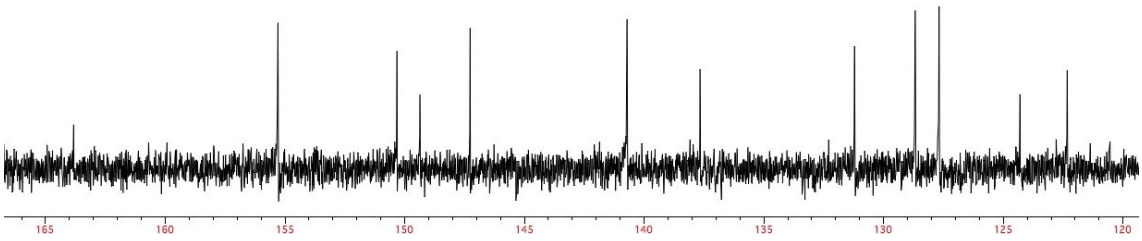

Figure S7. *fac*-[Re(**bipy**)$(CO)_3$(**2-PTZ**)]: ^{1}H-NMR spectrum **(**DMSO-*d*^{6}, 400 MHz, r.t.).

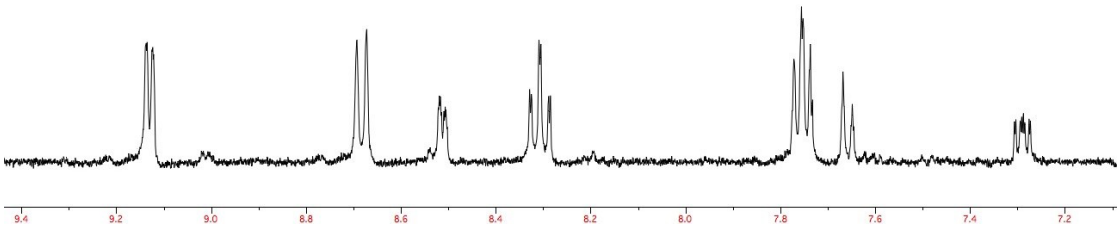

Figure S8. *fac*-[Re(**bipy**)$(CO)_3$(**2-PTZ**)]: ^{13}C-NMR spectrum **(**DMSO-*d*^{6}, 100 MHz, r.t.).

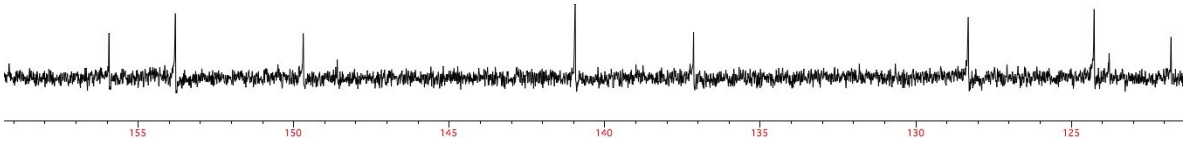

Figure S9. [**Re-(2-PTZ)-Cu**]$^{+}$: ^{1}H-NMR spectrum (CDCl$_3$, 400 MHz, r.t.).

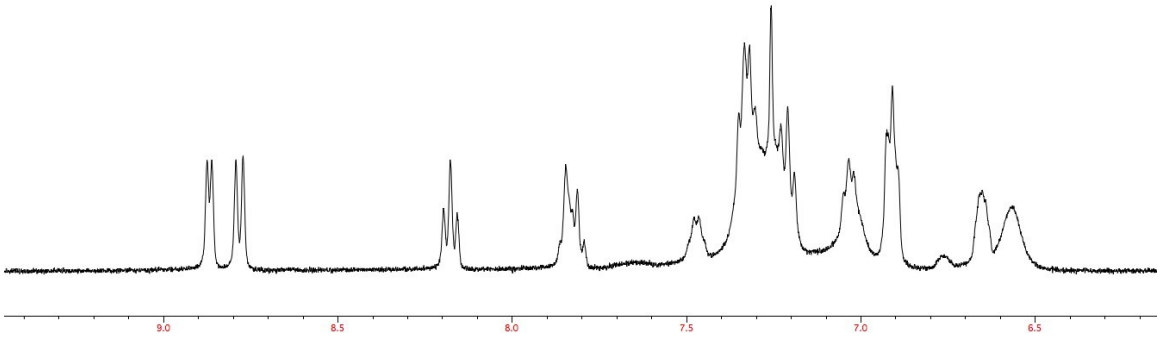

Figure S10. [**Re-(2-QTZ)-Cu**]$^{+}$: ^{1}H-NMR spectrum (CDCl$_3$, 400 MHz, r.t.).

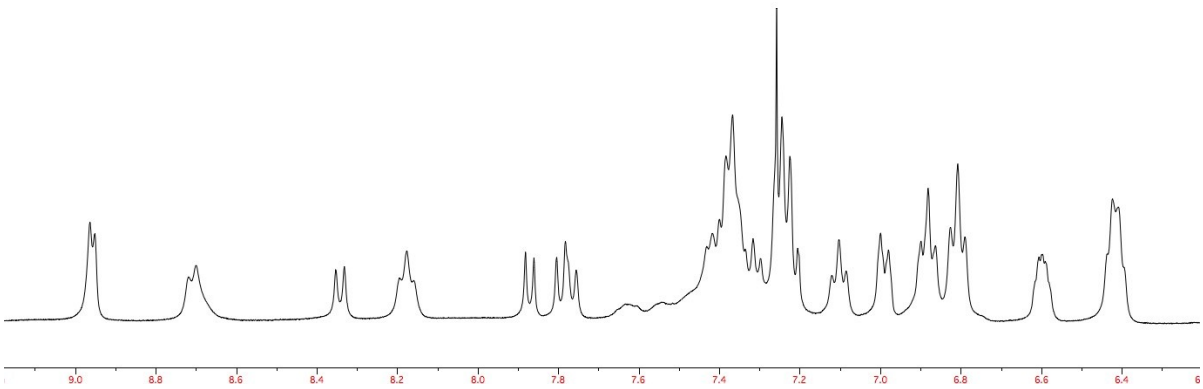

Absorption and Emission spectra

Figure S11. Absorption spectra of *fac*-[Re(**phen**)$(CO)_3$(**2-QTZ**)] (blue line) and *fac*-[Re(**phen**)$(CO)_3$(**2-PTZ**)] (black line), Solvent: CH_2Cl_2.

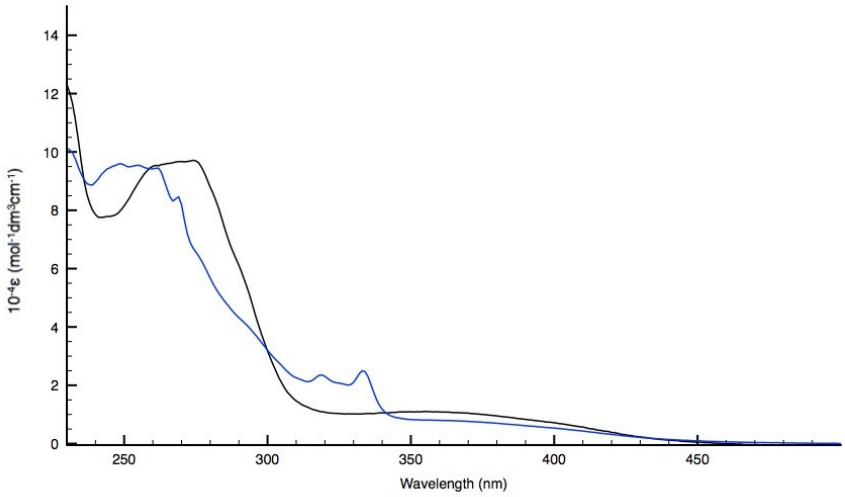

Figure S12. Absorption spectra of *fac*-[Re(**bipy**)$(CO)_3$(**2-QTZ**)] (blue) and *fac*-[Re(**phen**)$(CO)_3$(**2-PTZ**)] (black), Solvent: CH_2Cl_2.

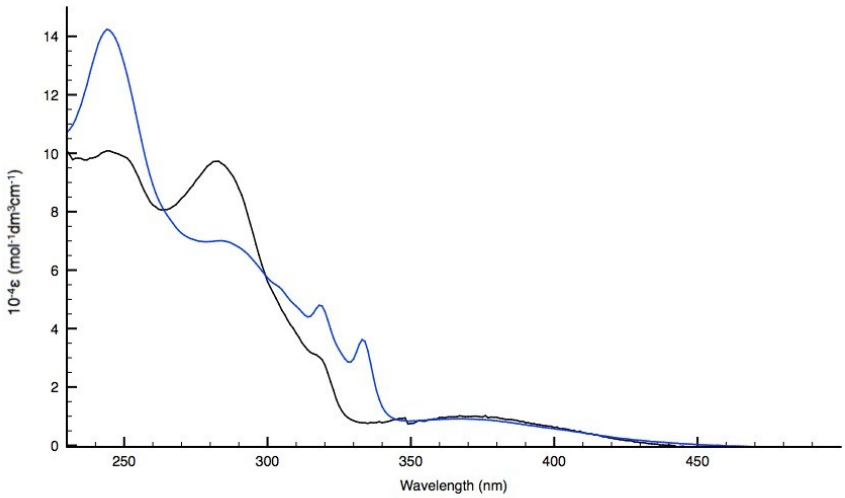

Figure S13. Normalized emission profiles of *fac*-[Re(**phen**)$(CO)_3$(**2-QTZ**)] 77K (blue) and 298K (red), Solvent: CH_2Cl_2.

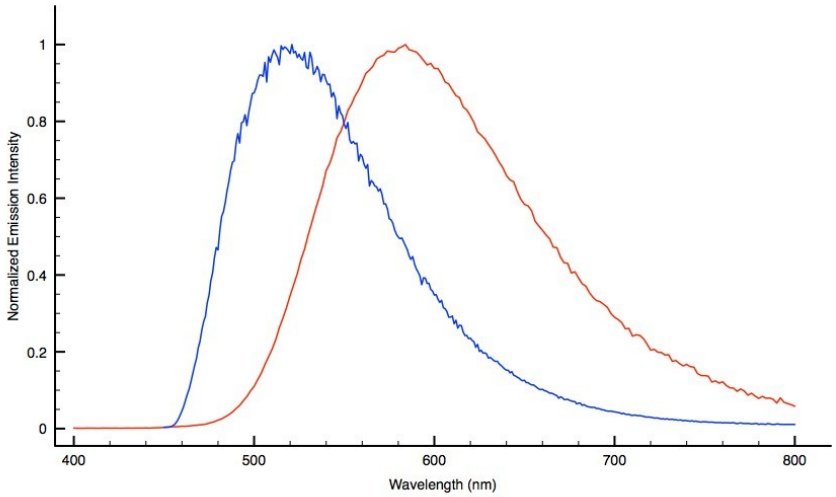

Figure S14. Normalized emission profiles of *fac*-[Re(**bipy**)$(CO)_3$(**2-QTZ**)] 77K (blue) and 298K (red), Solvent: CH_2Cl_2.

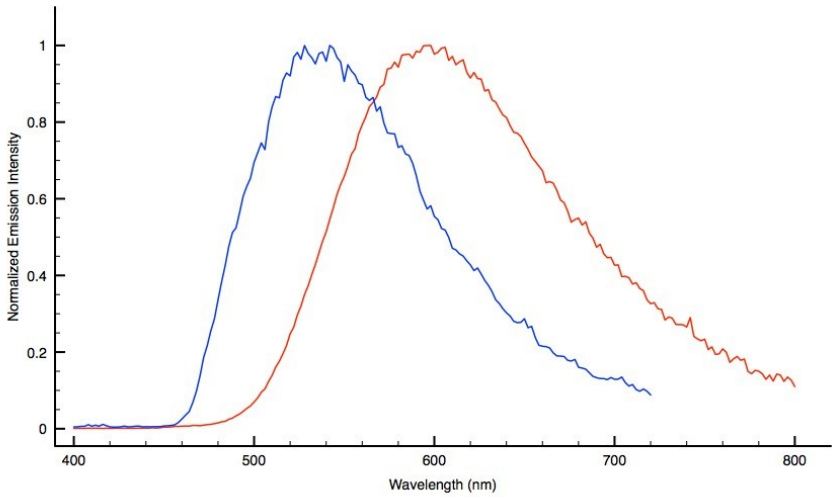

Figure S15. Normalized emission profiles of *fac*-[Re(**phen**)$(CO)_3$(**2-PTZ**)] 77K (blue) and 298K (red), Solvent: CH_2Cl_2.

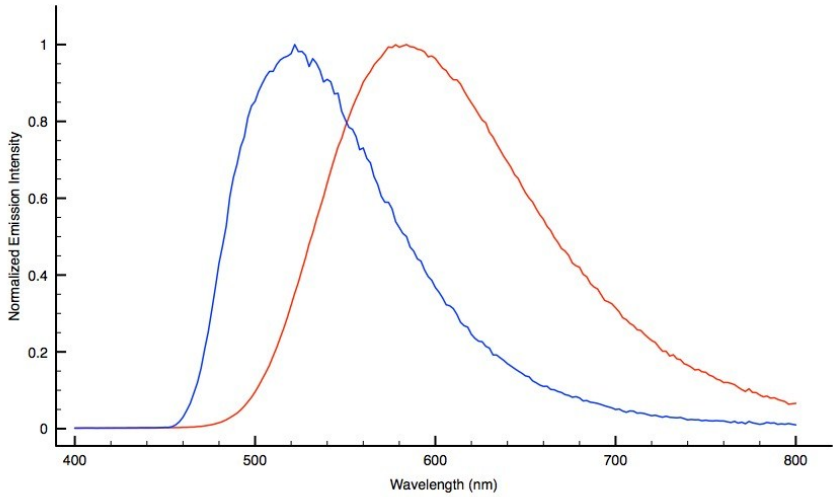

Figure S16. Normalized emission profiles of *fac*-[Re(**bipy**)$(CO)_3$(**2-PTZ**)] 77K (blue) and 298K (red), Solvent: CH_2Cl_2.

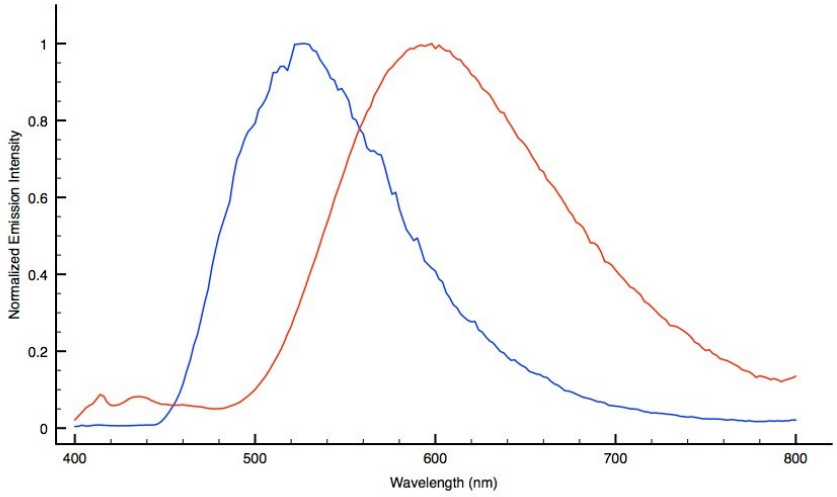

Table S2. Photophysical data for [**Re-(2-QTZ)-Cu**]$^+$ and [**Re-(2-PTZ)-Cu**]$^+$.

Complex	**Absorption (CH_2Cl_2)**	**Emission 298K (CH_2Cl_2)**		**Emission 298 K neat solid**	
	λ [nm]	λ	τ	λ	τ
	(10^{-4} ε) [M^{-1} cm^{-1}]	[nm]	[ns]	[nm]	[μs]
[Re-(2-QTZ)-Cu]$^+$	250(12.08), 282(6.07), 317(3.57), 338(2.13), 382(0.99)	597	n.d	562	12.0
[Re-(2-PTZ)-Cu]$^+$	249(7.03), 282(5.34), 319(2.44), 352(0.85)	590	n.d	518	1.7

Figure S17. Absorption profiles of [**Re-(2-QTZ)-Cu**]$^+$, black line, [**Re-(2-PTZ)-Cu**]$^+$, blue line.

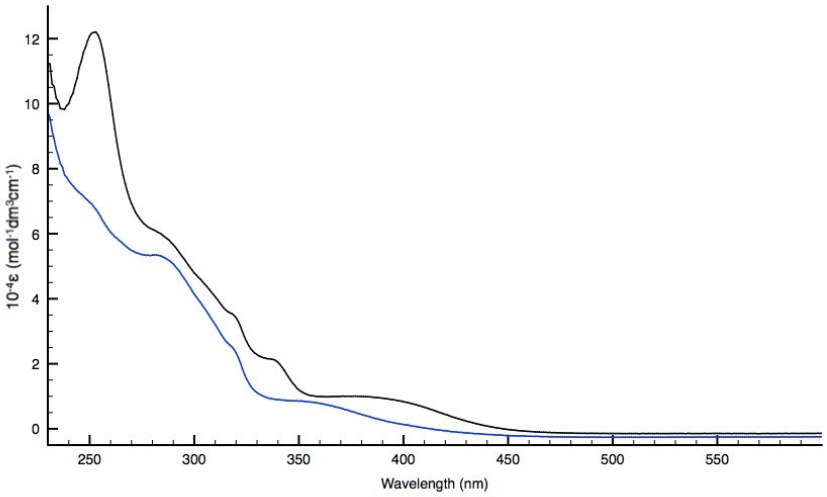

Figure S18. Emission profiles of [**Re**-(**2-QTZ**)-**Cu**]$^{+}$298K, (black line) and *fac*-[Re(**bipy**)$(CO)_3$(**2-QTZ**)] 298K (blue line). Solvent: CH_2Cl_2.

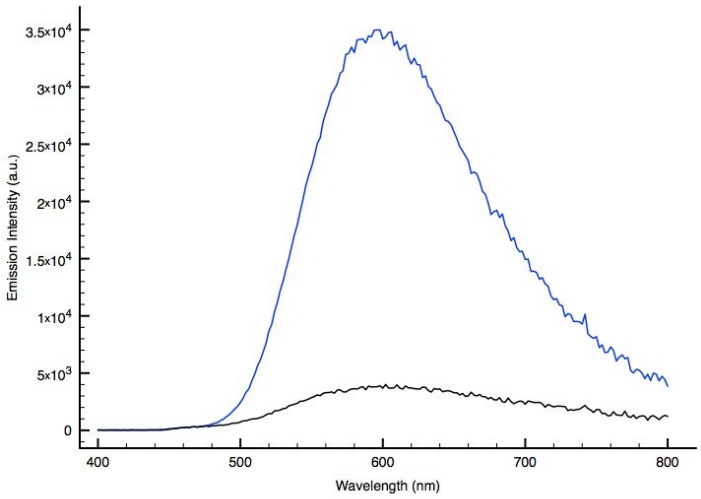

Figure S19. Emission spectra of [**Re**-(**2-PTZ**)-**Cu**]$^{+}$298K, (black line) and *fac*-[Re(**bipy**)$(CO)_3$(**2-PTZ**)] 298K (blue line). Solvent: CH_2Cl_2.

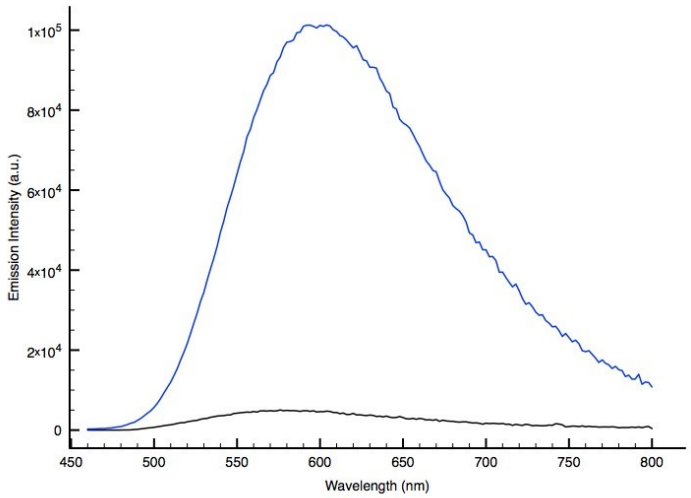

Figure S20. Emission spectrum of [**Re**-(**2-QTZ**)-**Cu**]$^{+}$, solid state, 298 K.

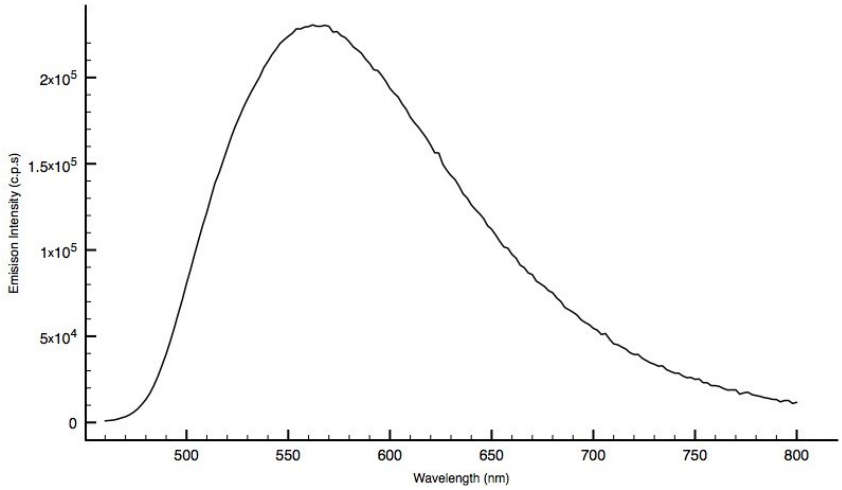

Figure S21. Emission profile of [**Re**-(**2-PTZ**)-**Cu**]$^{+}$, solid state, 298 K.

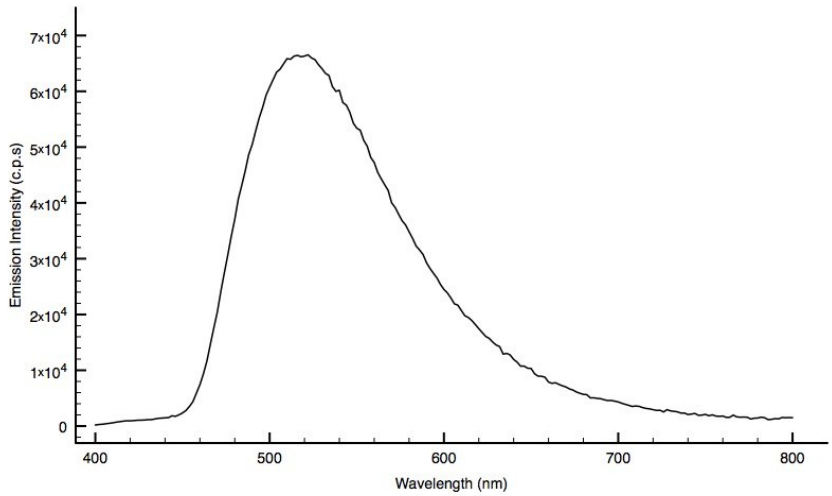

Effects of binding to metal cations: Absorption spectra, emission titrations and lifetime decays

Figure S22. Absorption spectra of *fac*-[Re(**phen**)$(CO)_3$(**2-QTZ**)] (black line), *fac*-[Re(**phen**)$(CO)_3$(**2-QTZ**)] + Zn^{2+} (blue line) *fac*-[Re(**phen**)$(CO)_3$(**2-QTZ**)] +Cd^{2+} (red line), *fac*-[Re(**phen**)$(CO)_3$(**2-QTZ**)] +Cu^{2+} (green line). Solvent: CH_3CN.

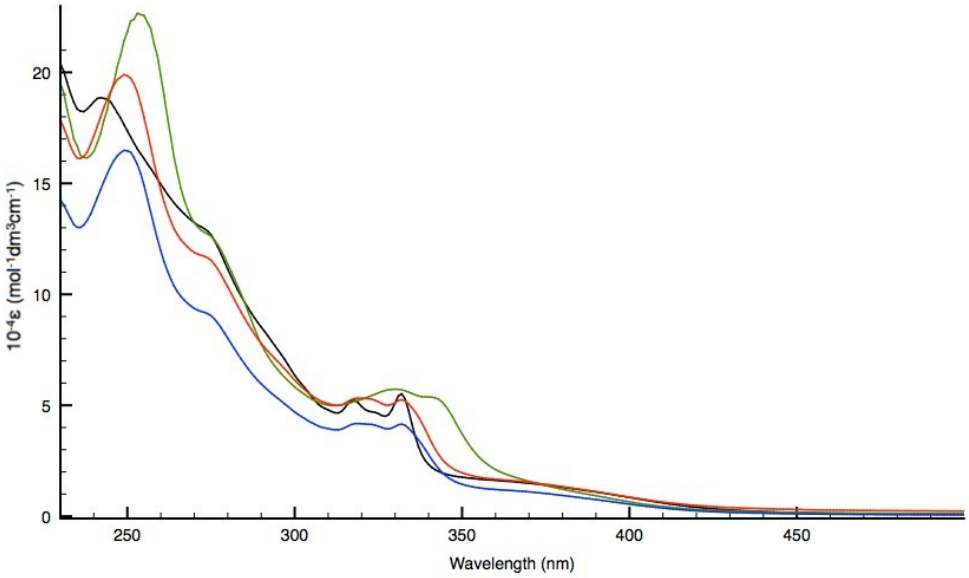

Figure S23. Absorption Spectra of *fac*-[Re(**bipy**)$(CO)_3$(**2-QTZ**)] (black), *fac*-[Re(**bipy**)$(CO)_3$(**2-QTZ**)] + Zn^{2+} (blue), *fac*-[Re(**bipy**)$(CO)_3$(**2-QTZ**)] +Cd^{2+} (red), *fac*-[Re(**bipy**)$(CO)_3$(**2-QTZ**)] +Cu^{2+} (green). Solvent: CH_3CN.

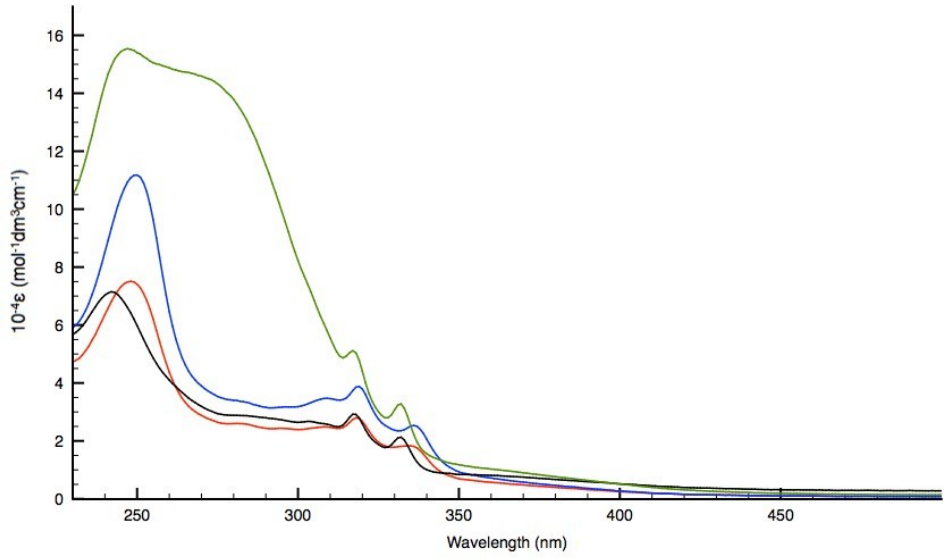

Figure S24. Absorption Spectra of *fac*-[Re(phen)$(CO)_3$(2-PTZ)] (black), *fac*-[Re(phen)$(CO)_3$(**2-PTZ**)]+ Zn^{2+} (blue), *fac*-[Re(**phen**)$(CO)_3$(**2-PTZ**)]+Cd^{2+} (red), *fac*-[Re(**phen**)$(CO)_3$(**2-PTZ**)] +Cu^{2+} (green). Solvent: CH_3CN.

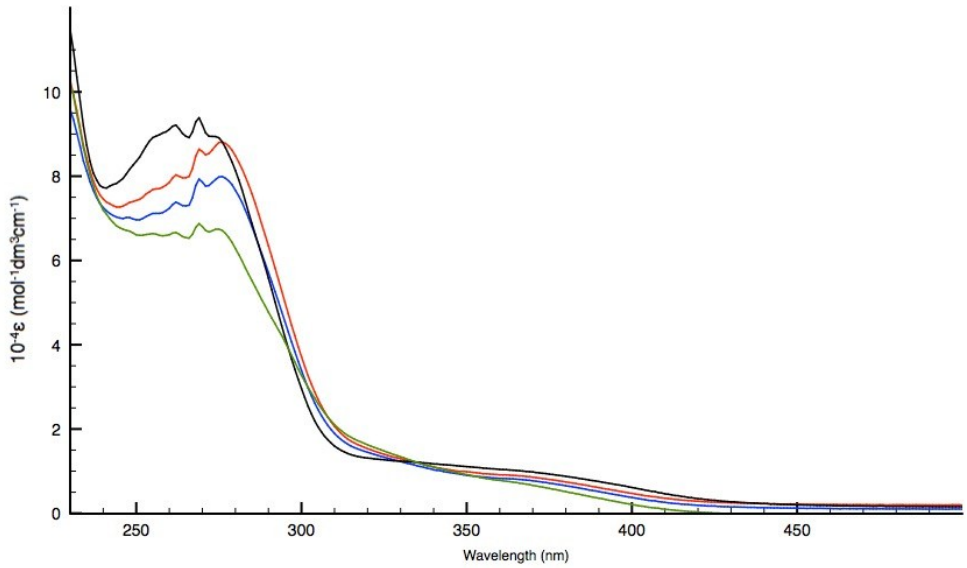

Figure S25. Absorption Spectra of *fac*-[Re(**bipy**)$(CO)_3$(**2-PTZ**)] (black), *fac*-[Re(**bipy**)$(CO)_3$(**2-PTZ**)] + Zn^{2+} (blue), *fac*-[Re(**bipy**)$(CO)_3$(**2-PTZ**)] +Cd^{2+} (red), *fac*-[Re(**bipy**)$(CO)_3$(**2-PTZ**)] +Cu^{2+} (green). Solvent: CH_3CN.

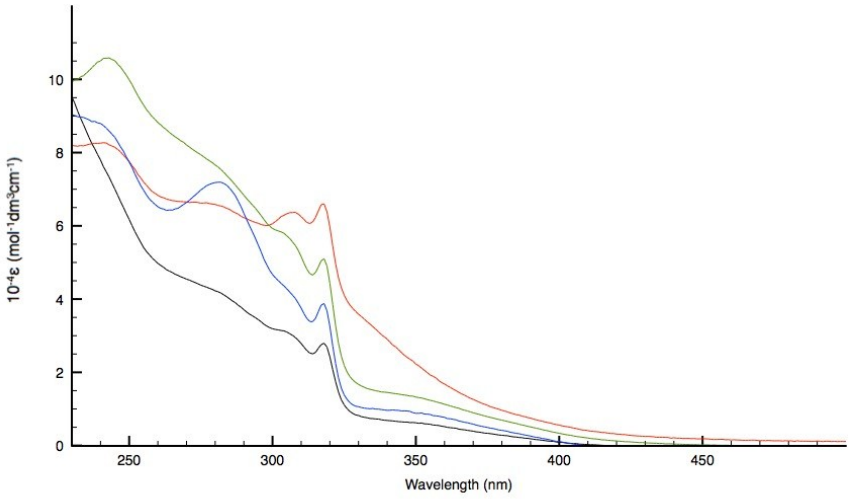

Emission titrations

Figure S26. Steady-state emission spectra showing the blue shift and the increase of emission intensity of *fac*-[Re(**phen**)$(CO)_3$(**2-QTZ**)] (1,55*10^{-4}M), 10 µL aliquots for 20 additions with $Zn(ClO_4)_2$ in CH_3CN, 5,37*10^{-4}M;

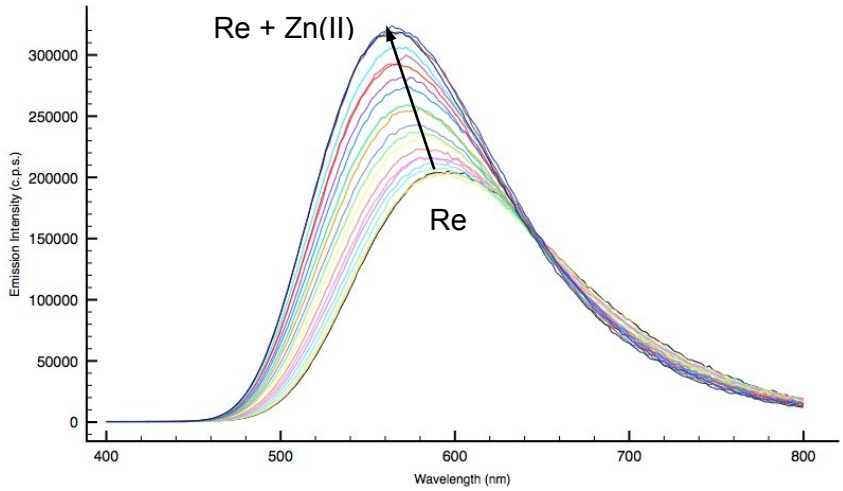

Figure S27. Steady-state emission spectra showing the blue shift and the increase of emission intensity of *fac*-[Re(**phen**)$(CO)_3$(**2-QTZ**)] (1,55*10^{-4}M), 10 µL aliquots for 60 additions with $Cd(ClO_4)_2$ in CH_3CN, 2,38*10^{-4}M;

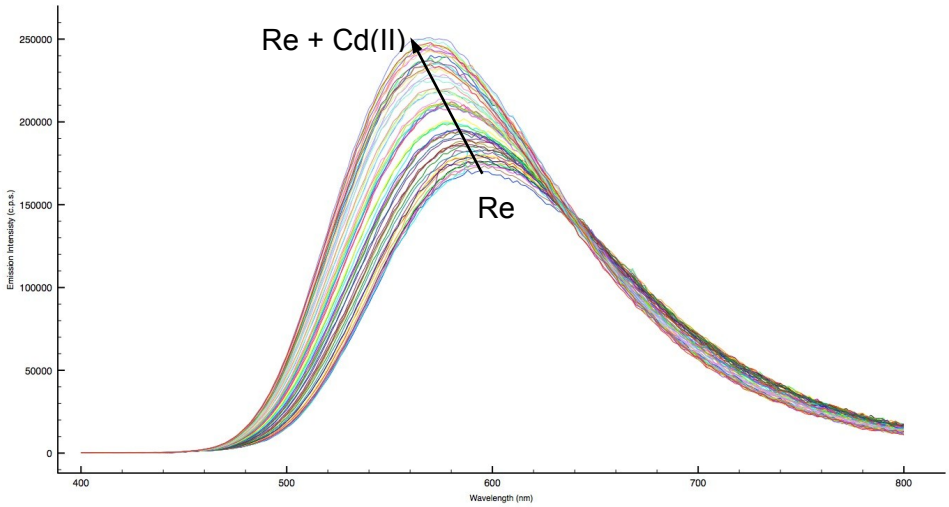

Figure S28. Steady-state emission spectra showing the suppression of radiative processes of *fac*-[Re(**phen**)$(CO)_3$(**2-QTZ**)] ($1{,}55*10^{-4}$M), 5 µL aliquots for 20 additions with $Cu(ClO_4)_2$ in CH_3CN, $2{,}69*10^{-4}$M;

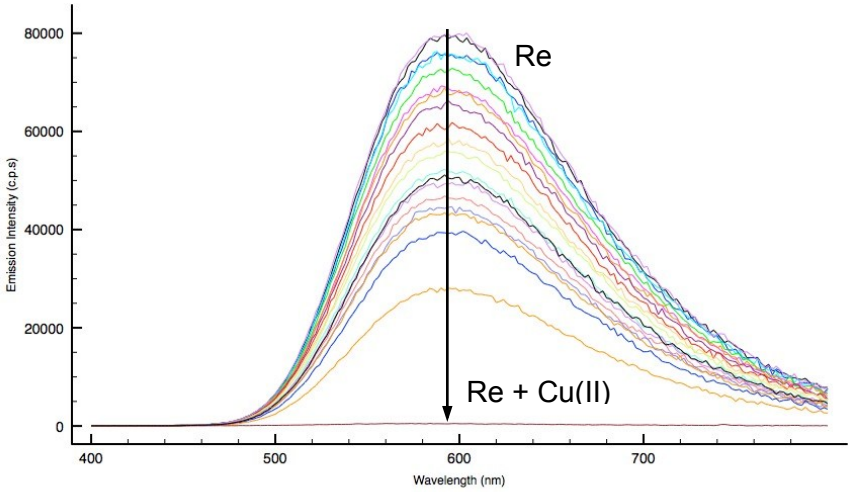

Figure S29. Steady-state emission spectra showing the blue shift and the increase of emission intensity of *fac*-[Re(**phen**)$(CO)_3$(**2-PTZ**)] (1,68*10^{-4}M), 10 µL aliquots for 28 additions with $Zn(ClO_4)_2$ in CH_3CN, 5,37*10^{-4}M;

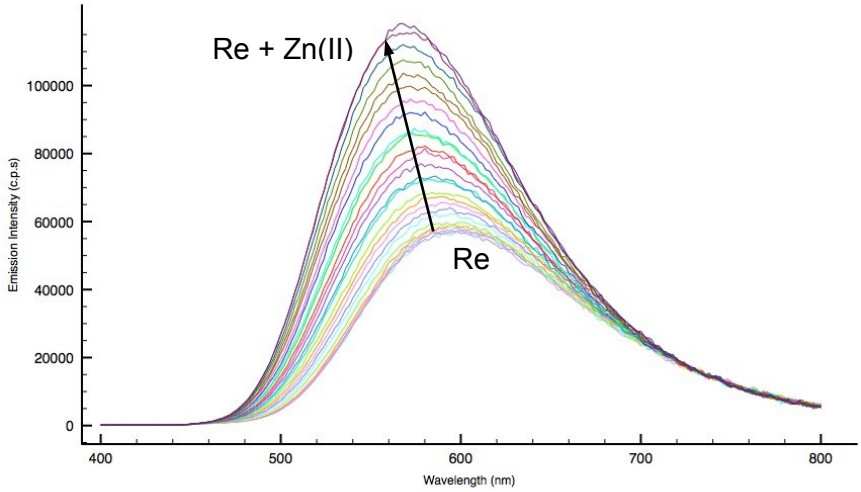

Figure S30. Steady-state emission spectra showing the blue shift and the increase of emission intensity of *fac*-[Re(**phen**)$(CO)_3$(**2-PTZ**)] (1,68*10^{-4}M), 10 µL aliquots for 60 additions with $Cd(ClO_4)_2$ in CH_3CN, 2,38*10^{-4}M;

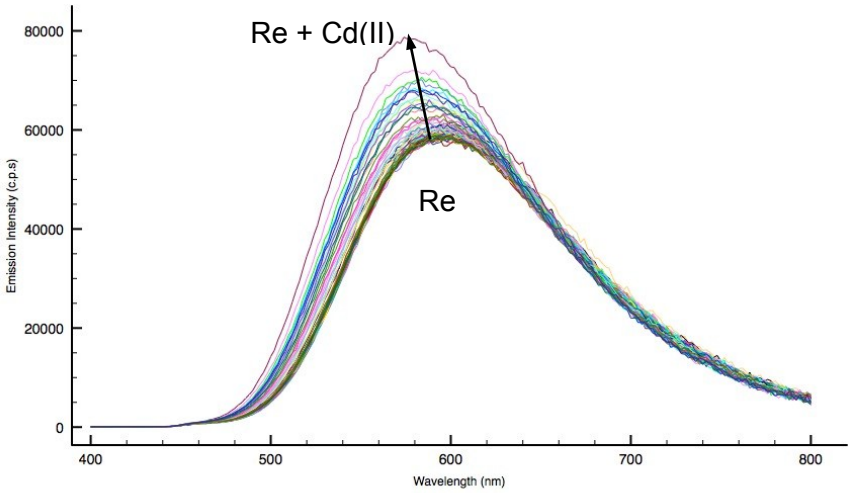

Figure S31. Steady-state emission spectra showing the suppression of radiative processes of *fac*-[Re(**phen**)$(CO)_3$(**2-PTZ**)] (1,68*10^{-4}M), 100 µL aliquots for 5 additions with $Cu(ClO_4)_2$ in CH_3CN, 2,69*10^{-4}M;

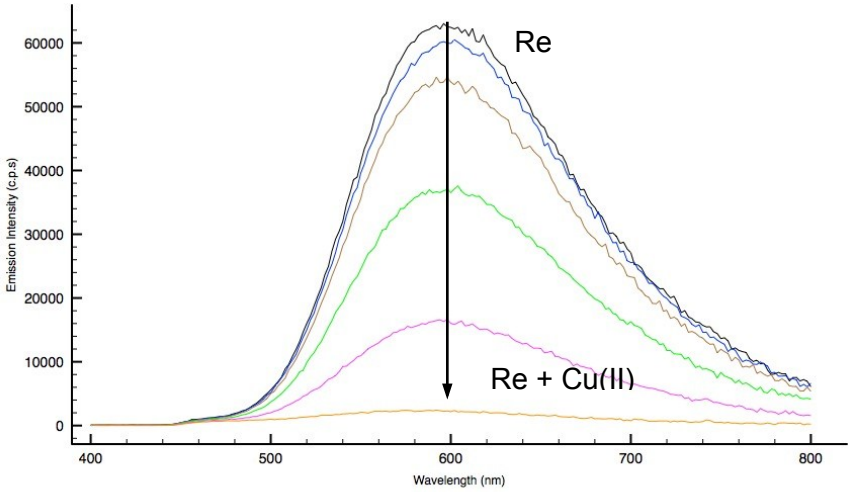

Figure S32. Comparison of lifetime decays of *fac*-**[**Re(**phen**)$(CO)_3$(**2-PTZ**)] denoted as "**Re**", in the absence (black trace) and in the presence of Cd(II) (red trace) and Zn(II) (blue trace).

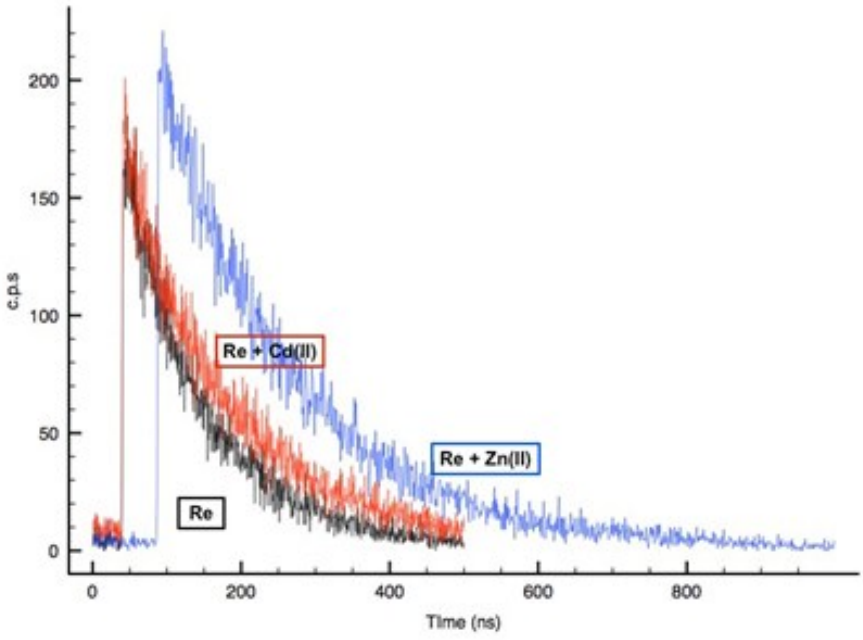

Figure S33. Steady-state emission spectra showing the blue shift and the increase of emission intensity of *fac*-[Re(**bipy**)$(CO)_3$(**2-QTZ**)] ($1{,}61*10^{-4}$M), 10 µL aliquots for 20 additions with $Zn(ClO_4)_2$ in CH_3CN, $5{,}37*10^{-4}$M;

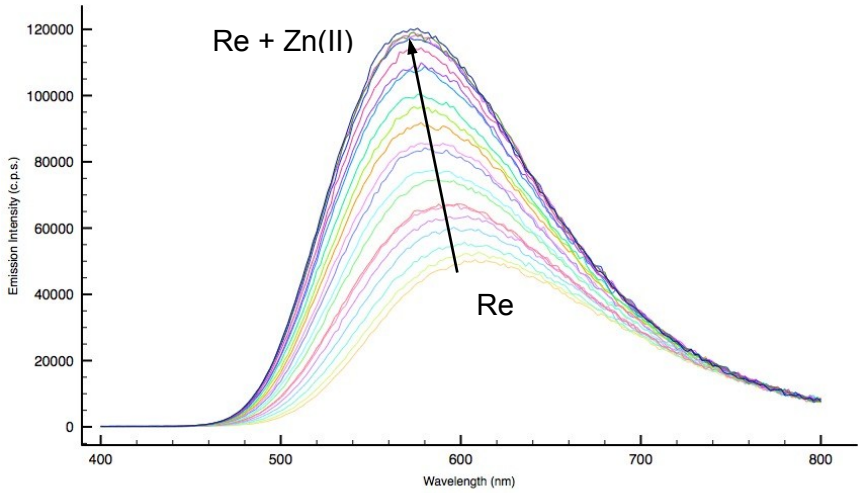

Figure S34. Steady-state emission spectra showing the blue shift and the increase of emission intensity of *fac*-[Re(**bipy**)$(CO)_3$(**2-QTZ**)] ($1{,}61*10^{-4}$M), 10 µL aliquots for 60 additions with $Cd(ClO_4)_2$ in CH_3CN, $2{,}38*10^{-4}$M;

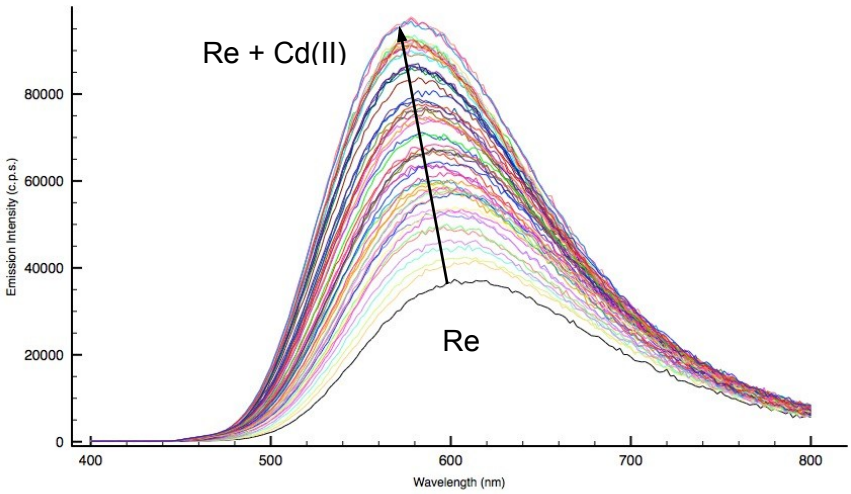

Figure S35. Steady-state emission spectra showing the suppression of radiative processes of *fac*-[Re(**bipy**)$(CO)_3$(**2-QTZ**)] (1,61*10^{-4}M), 100 µL aliquots for 3 additions with $Cu(ClO_4)_2$ in CH_3CN, 2,69*10^{-4}M;

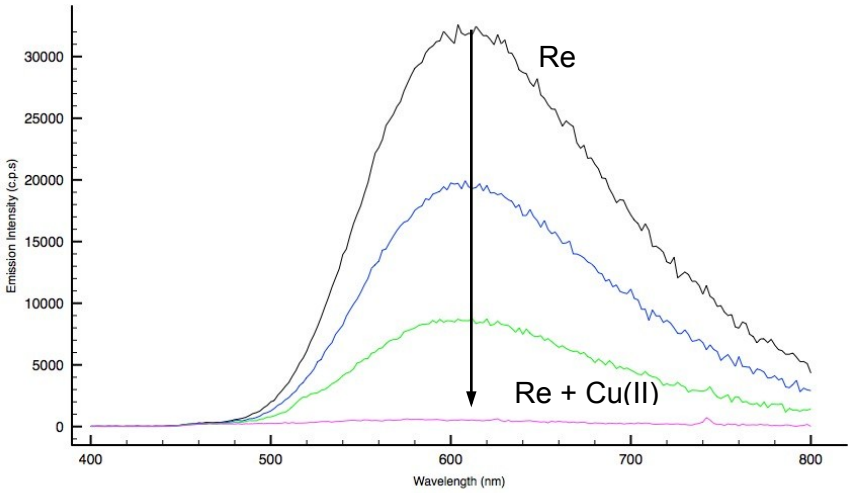

Figure S36. Comparison of lifetime decays of *fac*-**[**Re(**bipy**)$(CO)_3$(**2-QTZ**)] denoted as "**Re**", in the absence (black trace) and in the presence of Cd(II) (red trace) and Zn(II) (blue trace).

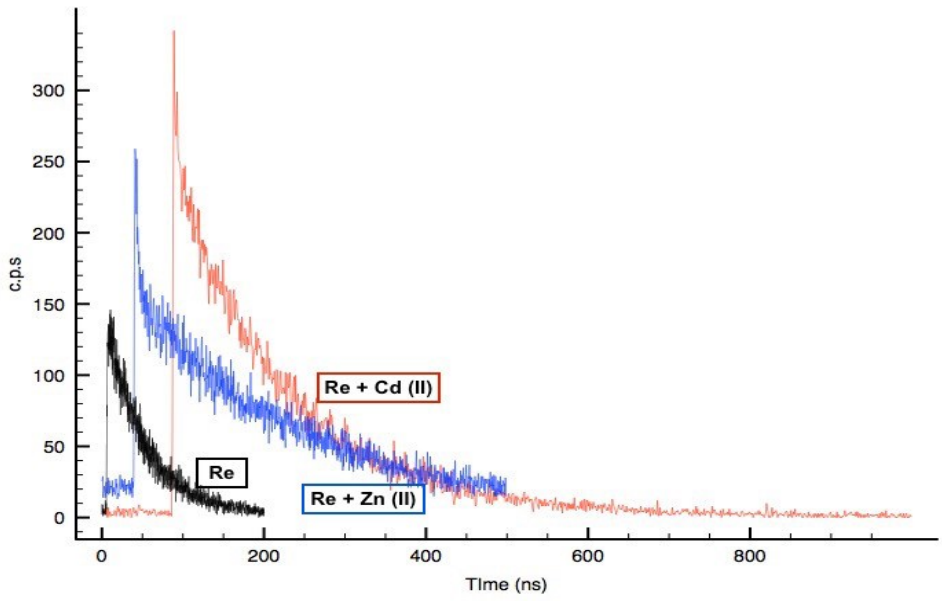

Figure S37. Steady-state emission spectra showing the blue shift and the increase of emission intensity of *fac*-[Re(**bipy**)$(CO)_3$(**2-PTZ**)] (1,75*10^{-4}M), 10 µL aliquots for 23 additions with $Zn(ClO_4)_2$ in CH_3CN, 5,37*10^{-4}M**;**

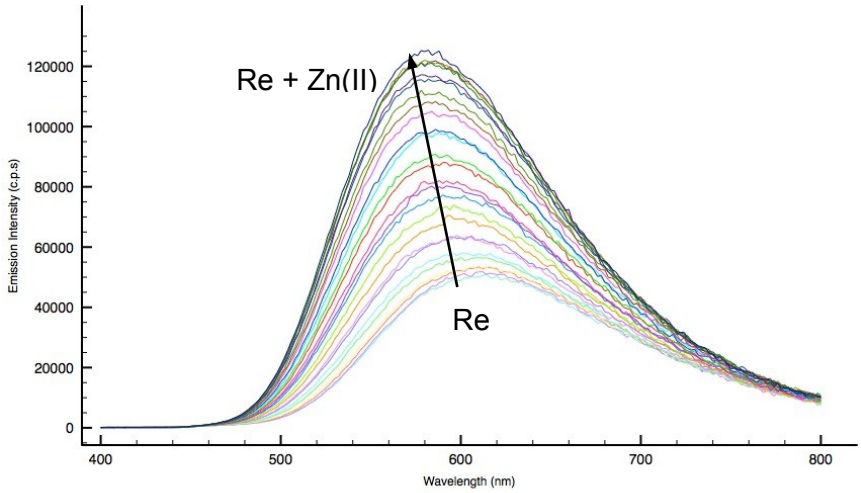

Figure S38. Steady-state emission spectra showing the blue shift and the increase of emission intensity of *fac*-[Re(**bipy**)$(CO)_3$(**2-PTZ**)] (1,75*10^{-4}M), 10 µL aliquots for 50 additions with $Cd(ClO_4)_2$ in CH_3CN, 2,38*10^{-4}M;

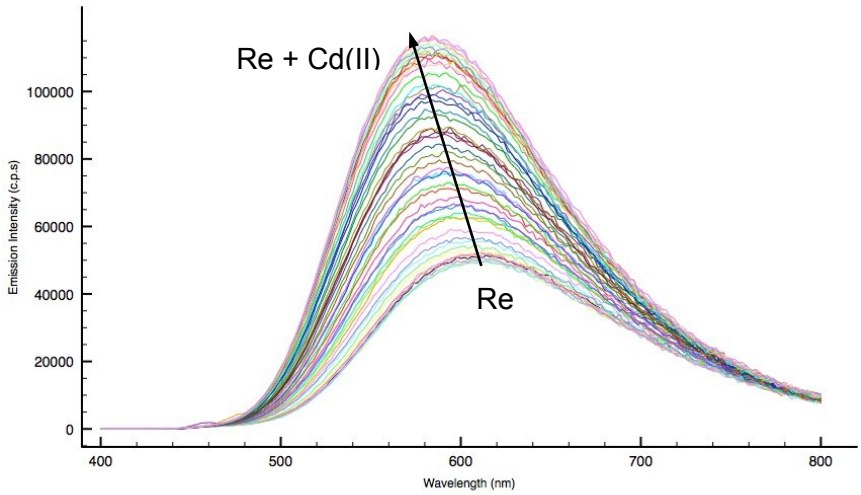

Figure S39. Steady-state emission spectra showing the suppression of radiative processes of *fac*-[Re(**bipy**)$(CO)_3$(**2-PTZ**)] ($1{,}75*10^{-4}$M), 100 μL aliquots for 6 additions with $Cu(ClO_4)_2$ in CH_3CN, $2{,}69*10^{-4}$M;

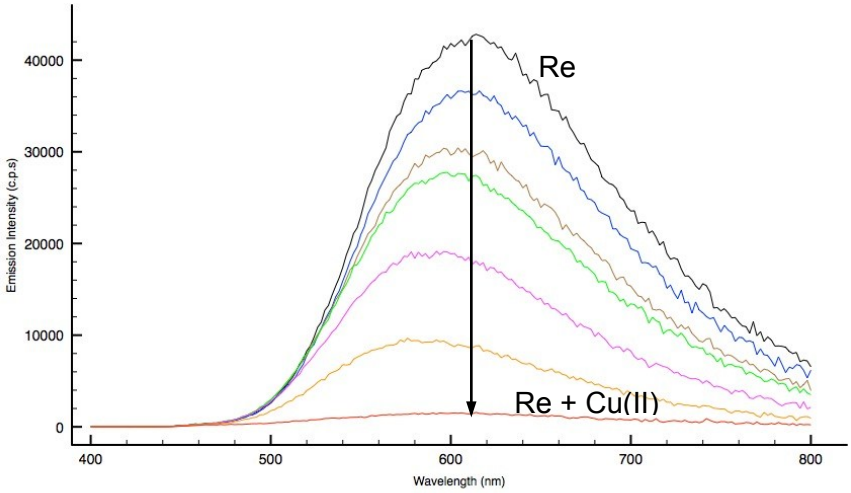

Figure S40. Comparison of lifetime decays of *fac*-**[**Re(**bipy**)$(CO)_3$(**2-PTZ**)] denoted as "**Re**", in the absence (black trace) and in the presence of Cd(II) (red trace) and Zn(II) (blue trace).

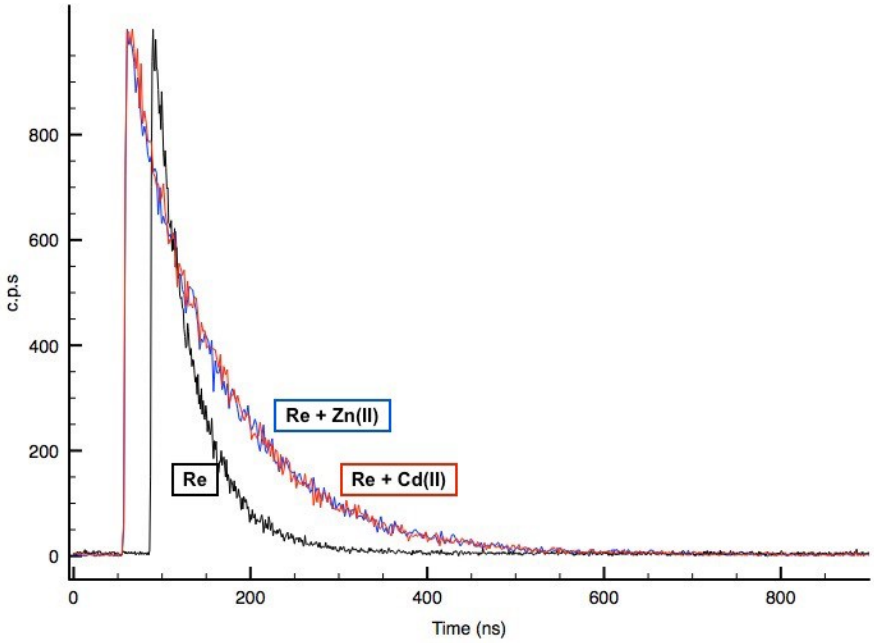

Figure S41. *fac*-[Re(**bipy**)$(CO)_3$(**2-QTZ**)], CH_3CN, 10^{-5}M

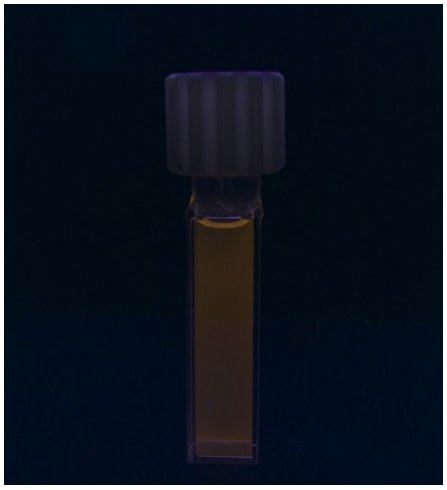

Figure S42. *fac*-[Re(**bipy**)$(CO)_3$(**2-QTZ**)] + Zn^{2+}, CH_3CN, 10^{-5}M

Figure S43. *fac*-[Re(**bipy**)$(CO)_3$(**2-QTZ**)] + Cd^{2+}, CH_3CN, 10^{-5}M

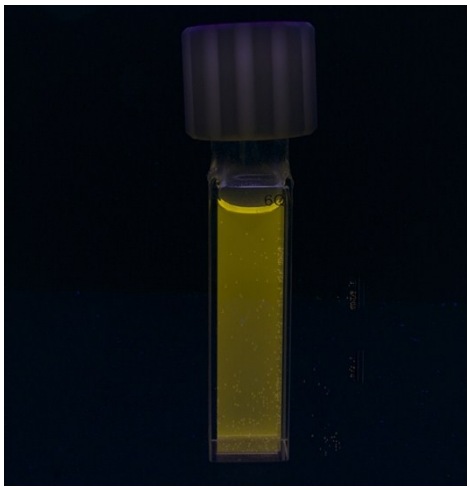

Figure S44. Stern Volmer Plot of *fac*-[Re(**phen**)$(CO)_3$(**2-QTZ**)]

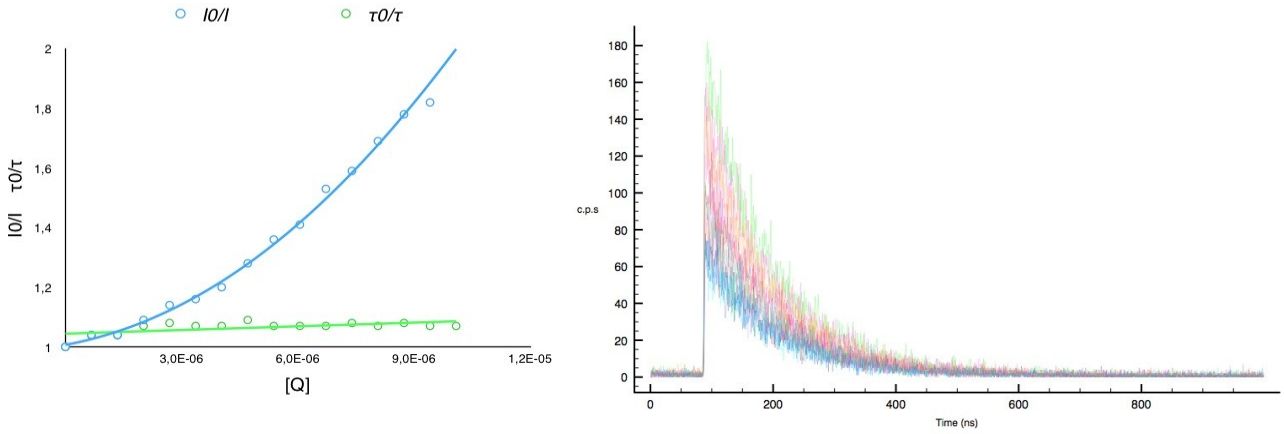

The upward curvature of I_0/I vs $[Cu^{2+}]$ (denoted as "[Q]" in figure S45, left) and the straight line of τ_0/τ vs $[Cu^{2+}]$ suggests that both static and dynamic quenching are occurring, as confirmed by the substantially unchanged lifetime values recorded after the addition of each Cu^{2+} aliquot. (figure S45, right)

Table S3. Stern Volmer Data of *fac*-[Re(**phen**)$(CO)_3$(**2-QTZ**)]

V added (µL)	**I0/I**[a]	**τo/τ**[a]	**[Cu^{2+}]** (mol/L)
0	1	1	0
5	1,04	1,039	$6{,}725*10^{-07}$
10	1,04	1,039	$1{,}345*10^{-06}$
15	1,09	1,07	$2{,}0175*10^{-06}$
20	1,14	1,08	$2{,}69*10^{-06}$
25	1,16	1,07	$3{,}3625*10^{-06}$
30	1,20	1,07	$4{,}035*10^{-06}$
35	1,28	1,09	$4{,}7075*10^{-06}$
40	1,36	1,07	$5{,}38*10^{-06}$
45	1,41	1,07	$6{,}0525*10^{-06}$
50	1,53	1,07	$6{,}725*10^{-06}$
55	1,59	1,08	$7{,}3975*10^{-06}$
60	1,69	1,07	$8{,}07*10^{-06}$
65	1,78	1,08	$8{,}7425*10^{-06}$
70	1,82	1,07	$9{,}415*10^{-06}$
75	2,04	1,07	$1{,}0088*10^{-05}$

[a]:I_0/I = Integral of the Emission spectrum of free *fac*-[Re(**phen**)$(CO)_3$(**2-QTZ**)] (I_0) over the Integral of the emission spectrum of the complex after the addition of $[Cu^{2+}]$ (I). τ_0/τ = Decay time of free *fac*-[Re(**phen**)$(CO)_3$(**2-QTZ**)] (τ_0) over the decay time of the complex after the addition of $[Cu^{2+}]$ (τ).

Table S4. Crystal data and collection details for *fac*-[Re(**bipy**)$(CO)_3$(**2-PTZ**)], *fac*-[Re(**phen**)$(CO)_3$(**2-PTZ**)]·CH_2Cl_2, *fac*-[Re(**phen**)$(CO)_3$(**2-QTZ**)]·$0.5CH_2Cl_2$, *fac*-[Re(**bipy**)$(CO)_3$(**2-PTZ**)(**CuPOP**)][BF_4]·$2Et_2O$ and *fac*-[Re(**bipy**)$(CO)_3$(**2-QTZ**)(**CuPOP**)][BF_4]·$1.67CH_2Cl_2$.

	***fac*-[Re(bipy)$(CO)_3$(2-PTZ)]**	***fac*-[Re(phen)$(CO)_3$(2-PTZ)]·CH_2Cl_2**	***fac*-[Re(phen)$(CO)_3$(2-QTZ)]·$0.5CH_2Cl_2$**
Formula	$C_{19}H_{12}N_7O_3Re$	$C_{22}H_{14}Cl_2N_7O_3Re$	$C_{25.5}H_{15}ClN_7O_3Re$
Fw	572.56	681.50	689.10
T, K	100(2)	100(2)	100(2)
λ, Å	0.71073	0.71073	0.71073
Crystal system	Triclinic	Orthorhombic	Orthorhombic
Space Group	$P\bar{1}$	*Pbca*	$P2_12_12_1$
a, Å	7.1047(9)	21.5431(8)	9.9769(7)
b, Å	8.6047(11)	9.3550(4)	21.4246(15)
c, Å	15.5783(19)	23.2990(9)	22.3643(14)
α, °	84.8870(10)	90	90
β, °	79.2250(10)	90	90
γ, °	89.4700(10)	90	90
Cell Volume, $Å^3$	931.8(2)	4695.6(3)	4780.4(6)
Z	2	8	8
D_c, g cm^{-3}	2.041	1.928	1.915
μ, mm^{-1}	6.559	5.444	5.241
F(000)	548	2624	2664
Crystal size, mm	0.15×0.12×0.11	0.23×0.19×0.14	0.19×0.13×0.12
θ limits, °	2.38–27.00	1.75–27.10	1.32–27.00
Index ranges	-9≤ h ≤ 9 -10≤ k ≤ 10 -19≤ l ≤19	-27≤ h ≤27 -11≤ k ≤ 11 -29≤ l ≤ 29	-12≤ h ≤12 -27≤ k ≤ 27 -28≤ l ≤ 28
Reflections collected	10194	41766	61366
Independent reflections	4014 [R_{int} = 0.0339]	5146 [R_{int} = 0.0485]	10436 [R_{int} = 0.0735]
Completeness to θ max	99.0%	100.0%	100.0%
Data / restraints /	4014 / 1 / 271	5146 / 0 / 316	10436 / 12 / 676

parameters			
Goodness on fit on F^2	1.101	1.080	1.024
R_1 ($I > 2\sigma(I)$)	0.0314	0.0239	0.0301
wR_2 (all data)	0.0765	0.0558	0.0574
Largest diff. peak and hole, e Å^{-3}	1.936 / –0.989	1.695 / –0.945	1.404 / –1.266

	***fac*-[Re(bipy)(CO)$_3$(2-PTZ)(CuPOP)][BF$_4$]·2Et$_2$O**	***fac*-[Re(bipy)(CO)$_3$(2-QTZ)(CuPOP)][BF$_4$]·1.67CH$_2$Cl$_2$**
Formula	$C_{63}H_{60}BCuF_4N_7O_6P_2Re$	$C_{60.67}H_{45.33}BCl_{3.33}CuF_4N_7O_4P_2Re$
Fw	1409.67	1453.03
T, K	100(2)	100(2)
λ, Å	0.71073	0.71073
Crystal system	Triclinic	Triclinic
Space Group	$P\bar{1}$	$P\bar{1}$
a, Å	13.358(3)	19.7532(12)
b, Å	13.894(3)	21.2407(13)
c, Å	17.428(4)	21.6526(13)
α, °	73.596(3)	73.361(3)
β, °	89.985(3)	89.462(4)
γ, °	79.009(3)	86.973(4)
Cell Volume, Å^3	3041.0(12)	8692.1(9)
Z	2	6
D_c, g cm^{-3}	1.539	1.666
μ, mm^{-1}	2.460	2.731
F(000)	1420	4332
Crystal size, mm	0.18×0.15×0.12	0.19×0.15×0.12
θ limits, °	1.56–25.03	0.98–25.03
Index ranges	-15≤ h ≤15	-23≤ h ≤23

	-16≤ k ≤ 16 -20≤ l ≤ 20	-25≤ k ≤ 25 -25≤ l ≤ 25
Reflections collected	23738	125847
Independent reflections	10638 [R_{int} = 0.0564]	30668 [R_{int} = 0.1031]
Completeness to θ max	99.9%	99.8%
Data / restraints / parameters	10638 / 434 / 762	30668 / 78 / 2053
Goodness on fit on F^2	1.083	1.082
R_1 (I> 2σ(I))	0.0637	0.0743
wR_2 (all data)	0.1692	0.2212
Largest diff. peak and hole, e Å^{-3}	3.199 / –1.572	5.318 / –2.836